# Passive isothermalisation of an exothermic reaction in flow using a novel "Heat Pipe Oscillatory Baffled Reactor (HPOBR)"

J.R. McDonough[a†], A.N. Phan[a], D.A. Reay[a], A.P. Harvey[a]

[a]School of Chemical Engineering and Advanced Materials, Department of Science Agriculture and Engineering, Newcastle University, Newcastle upon Tyne, NE1 7RU
[†]Corresponding Author

**Abstract:** In this study, a heat pipe was integrated with a mesoscale oscillatory baffled reactor for the passive temperature control of an exothermic reaction. The thermal/chemical performance of this new Heat Pipe Oscillatory Baffled Reactor (HPOBR) was compared to a conventional jacketed OBR (JOBR) using central composite experiment designs for an imination reaction between benzaldehyde and n-butylamine, in the absence of solvent. The variables in the experimental designs were reactant net flow rate ($Re_n$ = 4–20), fluid oscillation intensity ($Re_o$ = 123–491) and heat pipe fill ratio ($FR$ = 11.5–26.5; methanol working fluid). In the JOBR, the fill ratio factor was replaced with jacket temperature (4–20$°C$). Both reactors were able to reduce the maximum reaction temperature below the butylamine boiling point in all experiments. Overall, a 20-fold reduction in reactant volume and 13-fold improvement in reaction rate were obtained in the HPOBR for this imination reaction, compared with the same reaction using a solvent. Advantages of the HPOBR demonstrated here are isothermal operation and passive thermal control. Both reactors offer accelerated reaction rates and the potential for screening exothermic reactions. The HPOBR is a novel reactor design that provides a new approach for achieving green chemistry through solventless operation.

**Keywords:** Heat pipe reactor, exothermic, temperature control, green chemistry, process intensification

## 1 Introduction

Performing reactions without solvent is an attractive option for achieving green chemistry because it enables large increases in reaction rates and reduced downstream purification requirements, leading to process intensification. However, one consequence of significantly enhanced reaction rates for exothermic reactions is increased energy release. A solution to this problem is the heat pipe, which has been proposed for use in such chemical reactors [1,2]. Heat pipes operate through the evaporation and condensation of a working fluid, and possess numerous desirable attributes: (1) isothermal behaviour allowing for hot spot removal, (2) high heat load capabilities, (3) fast response times, and (4) large operating ranges (based on working fluid selection) [1].

There are very few examples in the literature of heat pipe integration into chemical reactors. In one study, Löwe *et al* (2009) [3] mounted a heat pipe-based CPU cooler to a microreactor for the synthesis of an ionic liquid. They reported that the point of thermal runaway (reaction temperature exceeding the reactant boiling temperature) was shifted from a total reactant flow rate of 1.713 *mL/min* to 9.7 *mL/min* with the heat pipe cooler, and up to 20 *mL/min* with additional fan-assisted forced convection cooling. Later, Wong *et al* (2014) [4] used a heat pipe to thermally control the removal of CO from a mixture of CO/H2. Here, the temperature spike observed at the reactor inlet was lowered, while the downstream temperature increased. Another application that heat pipes have been used for in reactors is the separation of heat source and sink. For example, a recent heat pipe reformer for gasification separated the reformer from the combustion chamber using heat pipes, where the heat transfer rate directly impacted upon the process efficiency [5].

In this work, a two-phase closed thermosyphon (a heat pipe relying on gravity to transfer the liquid condensate) was integrated with a mesoscale oscillatory baffled reactor. The original concept was to use the heat pipe design to accelerate temperature screening in flow chemistry applications, however, the application of interest here was the synthesis of an exothermic reaction without solvent. The aim was to isothermalise the reactor, thereby preventing boiling of the reactants. The heat released

from the reaction boils the working fluid in the heat pipe, reducing the intensity of the inlet temperature spike. The working fluid vapour is then driven to the outlet side of the reactor by a vapour pressure difference where it condenses, releasing the energy to the downstream portion of the reaction mixture. The ideal response is an isothermal axial temperature profile of the reaction. The process can operate in two modes. The first involves no net energy removal from the reactor, just energy redistribution. The second involves some additional energy removal from the system, e.g. through forced convection cooling of the heat pipe condenser (but this is not explored here).

The case study employed in this work was imination: a nucleophilic addition of primary amines to carbonyl compounds (aldehydes/ketones). Imination is exothermic and reactions proceed via two steps. First, a hemiaminal, -C(OH)(NH)-, tetrahedral intermediate is formed via an addition-elimination reaction between an aldehyde/ketone and amine. Then, water is removed via dehydration from the intermediate to produce the imine.

Imine compounds have a wide range of applications. They notably appear in the synthesis of amine compounds through reductive amination and imine hydrogenation [6,7], and are found in the synthesis of enantiomerically pure chiral compounds. Patents involving unsaturated imines as sulphur scavengers for petroleum products [8], and aromatic imines as water-soluble sulphur scavengers from wastewater [9] are also reported. Along similar lines, imines have been used in polymer synthesis for the formation of chelating resins for the removal of heavy metal ions from wastewater [10,11] and have been employed in cycloaddition reactions [12]. Importantly, since imination is reversible, it exists as one of the reactions available in dynamic combinatorial chemistry [13,14].

Various green chemistry approaches have been reported for the synthesis of imines. For instance, the use of water as a solvent showed surprisingly high yields (65–97%) in the synthesis of many aryl-alkyl and aryl-aryl imines from aromatic aldehydes, without the use of catalysts and buffering agents [11]. Similarly, high stability and yields were obtained for a macrocyclic diimine in pure water [15]. However, Saggiomo and Luning [13] suggest these high yields occurred either during or after work-up of the imine for analysis. Instead, in the absence of any solvent they found the exothermic reaction between benzaldehyde and aniline could produce a yield of 95% [13]. Also in the absence of any solvent, a green chemistry approach using microwave irradiation produced yields of over 90% for aryl aldehydes and amines with reaction times of just 1–5 *min* [16].

The objective of this work is to demonstrate a combined green chemistry/intensification approach to imination in which no solvent is used, where thermal control is provided using a HPOBR at milli-fluidic scale. This paper explores the performance of the reactor using central composite experiment designs. The thermal response is measured with thermocouples while the imination reaction is monitored in real time at the outlet using Fourier Transform Infrared (FTIR) spectroscopy. Chemical analysis is performed using principal components analysis (PCA) and partial least squares regression (PLS).

The results of a similar benchmark experiment design in a jacketed OBR (JOBR) are also reported. The purpose of this benchmark was to compare the performance of the two reactor platforms. The HPOBR is designed specifically to operate passively and achieve isothermal behaviour through the boiling and condensation of a working fluid. In contrast, the JOBR represents the conventional cooling approach often adapted in lab scale reaction platforms, with cooling achieved via the continuous circulation of a cooling fluid with a much larger flow rate than the reaction. The goal of the comparison was to identify the key operational differences to better understand the advantages of the HPOBR.

## 2 Methodology
### 2.1 Reactor Geometries
#### 2.1.1 Heat Pipe Oscillatory Baffled Reactor (HPOBR)

A schematic of the HPOBR is shown in Figure 1a. The inner meso-OBR was constructed using a 370 *mm* length 1/4", 22-gauge stainless steel 316 tube, giving an inner diameter of 4.93 *mm* and 0.711 *mm* wall thickness. The annular heat pipe, operating as a two-phase closed thermosyphon, was 350 *mm* in length and was constructed using a 7/8", 20-gauge stainless steel 316 tube. This gave the annular region an inner diameter of 6.35 *mm* and outer diameter of 20.4 *mm*. This size was chosen because it closely matched the jacket diameter available for the JOBR, and also minimised fluid entrainment whilst maximising proximity of the bulk working fluid volume to the reactor wall. The

heat pipe was sealed by welding two 3 *mm* thick stainless steel 316 plates at the top and bottom of the annular region. The total volume of the annular heat pipe was 104 *mL*. Figure 2 conveys the intended operation of the HPOBR using a thermal resistance network diagram.

Helical baffles (7.5 *mm* pitch, 1.1 *mm* thickness) were used in the meso-OBR as they allowed for the incorporation of 4 type-K thermocouples (0.75 *mm* diameter) to measure the axial temperature profile of the reaction. This gave a total reactor volume of 6.9 *mL* and an average open flow area of 73% (defined as the average free-flow area to total area). This approach was chosen because it was found to be simpler than fitting the thermocouples through the meso-OBR wall. Here, the thermocouples could not be welded due to their size and the braze material available was incompatible with the butylamine reactant. Additionally, one of the intended applications of this reactor is screening. Therefore, a larger reactor diameter was not considered because of the higher necessary throughput and potential safety issues (regarding the reaction heat release). The external temperature was measured using 3 type-K thermocouples fitted to the outer edge of the heat pipe. To ensure good thermal contact, a thermal-compound paste (Antec Formula 7) was used and enclosed with a small strip of aluminium tape. The positions of these thermocouples are shown in Figure1.

The heat pipe was filled and drained through a 1/4" tube welded on to outer heat pipe surface. To maintain a vacuum during operation, a plug valve (Swagelok, SS-4P4T) was fitted to this filling tube. The position of this filling line is shown in Figure 1a.

The HPOBR was also equipped with a 1" diameter and 1.5" length 200 *W* band heater (Watlow). Contact with the heat pipe was made using a stainless steel collar and thermal compound (Antec Formula 7). The heater was controlled using a CAL9400 PID controller. Two additional type-K thermocouples were brazed onto the outside edge of the meso-OBR tube during construction at distances of 23 *mm* and 123 *mm* from the top (Figure 1a). The upper thermocouple was used with the temperature controller while the lower thermocouple acted as a reference. A final type-K thermocouple was embedded in the heater to measure the control response. All thermocouples were connected to an 8-channel data logger (TC-08) and the data recorded in PicoLog (depending on the experiment configuration, not all thermocouples were connected to the logger).

Three C3000 series syringe pumps (Tricontinent) were used to supply the reactant net flow rates and generate fluid oscillation. The syringe pumps were connected to a custom built Swagelok union that was positioned at the base of the meso-OBR tube via PTFE tubing. The union was created by welding one 1/4" tube cap, one 1/8" tube cap and three 1/16" tube caps together (all supplied by Swagelok) and drilling out the centre. As only two reactants were used in this study, the third 1/16" port was sealed. The reagents contacted 2 *cm* beyond the inlet of the meso-OBR at the start of the cooling zone as shown in Figure 1a.

*2.1.2 Jacketed Oscillatory Baffled Reactor (JOBR)*

The JOBR geometry was very similar to the HPOBR. The inner meso-OBR was a glass tube of length 370 *mm* with inner/outer diameters of 5 *mm* and 8 *mm* respectively. The meso-OBR tube housed the same stainless steel helical baffle/thermocouple arrangement as the HPOBR, as shown in Figure 1b. The jacket itself was 350 *mm* in length, leaving a 2 *cm* unjacketed region at the inlet to connect the custom Swagelok union. Whereas the HPOBR functions through evaporation and condensation of a working fluid, the JOBR relies on the continuous circulation of a cooling liquid in the annular space surrounding the reactor. Two cooling configurations are possible using a jacket. These are maintaining a constant jacket temperature whilst varying the flow rate, and maintaining a constant flow rate whilst varying the temperature. For this work, the latter option (variable temperature) was selected because this was seen as more intuitive for adjusting the jacket's thermal mass. The jacket contained de-ionised water that was cooled/heated using a refrigerated bath (VWR, MX7LR-20, low profile). The bath had a working volume of 7 *L* and delivered a capacity of 11.9 *L/min*.
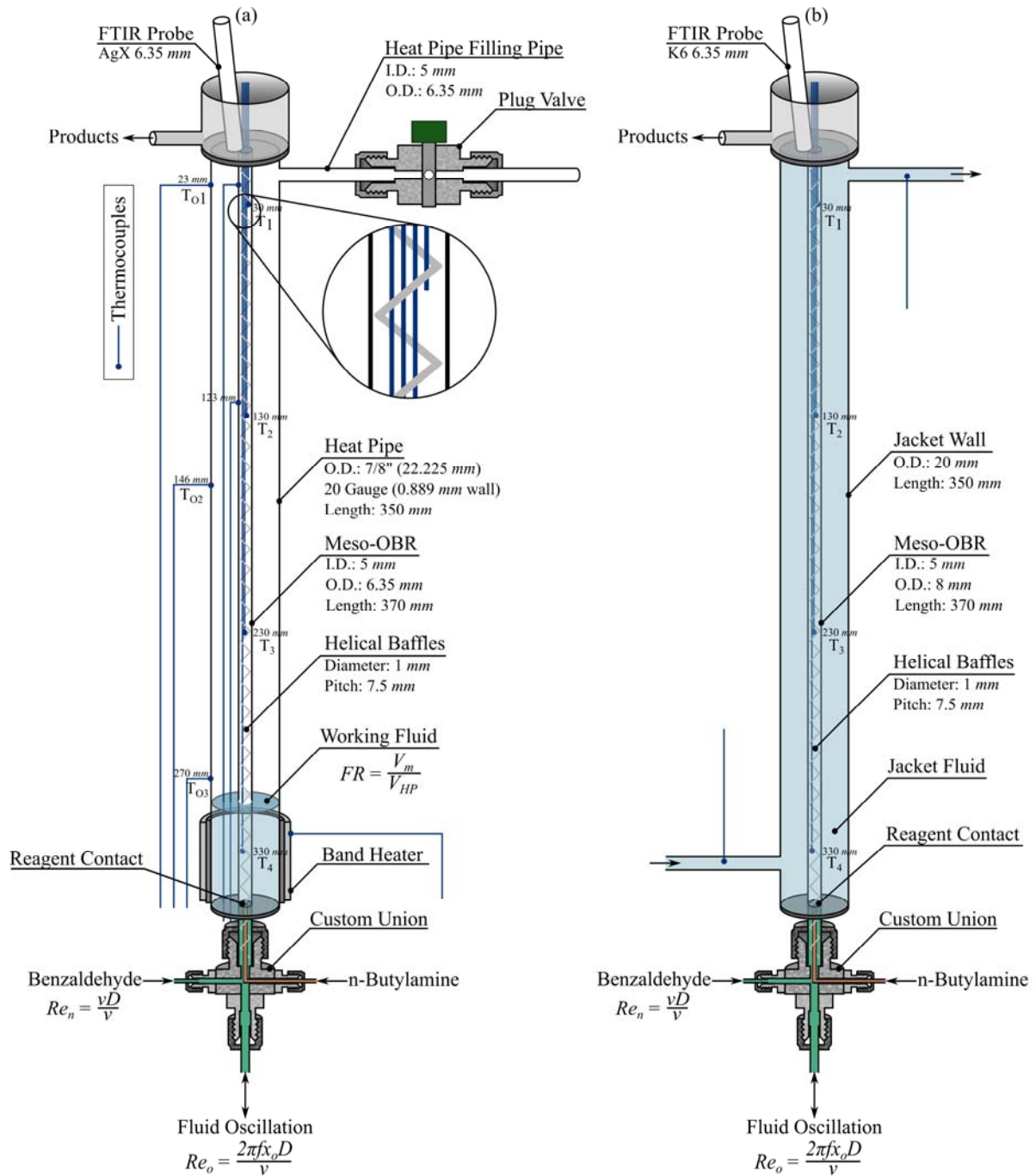
*Figure 1 – Schematic of the (a) HPOBR and (b) JOBR; positions of the thermocouples are defined from the top of the meso-OBR tube*
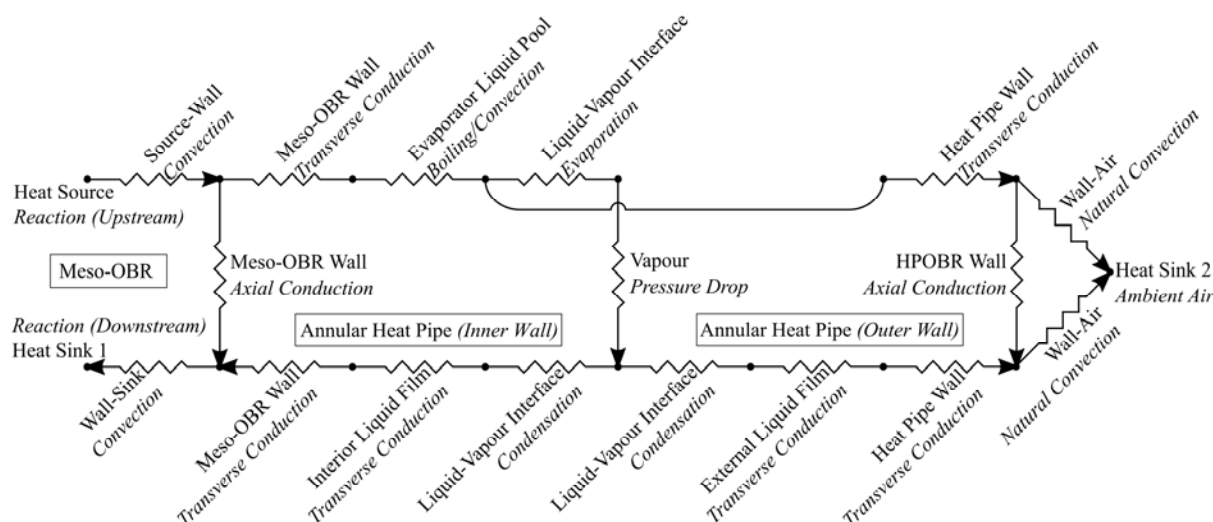
*Figure 2 – Heat transfer resistance network diagram for the HPOBR*

### 2.1.3 Fluid Mechanics

Meso-OBRs containing helical baffles produce a wide operating window for plug flow [17]. Here, the fluid mechanics are governed by the formation of vortices upon each flow reversal [18] as well as the presence of swirling flow which aids the minimisation of axial dispersion [17]. Expectedly, the addition of thermocouples to the baffles alters the mixing behaviour. To verify that plug flow was achievable with the current arrangement, standard tracer pulse experiments were performed for a variety of mixing conditions to evaluate the effective number of tanks-in-series. The same method as previous studies was used [17].

It was found that a high degree of plug flow ($N \geq 40$) was attainable for the majority of conditions used ($Re_n$ = 1.5–20, $x_o$ = 1–4 *mm* and $f$ = 2–10 *Hz*). In comparison, conventional helical baffles produce plug flow behaviour in the range of $20 < N < 40$ for similar oscillation conditions for net flows of $2.55 < Re_n < 7.2$ [17]. Addition of the thermocouples within the helical baffles leads to increased flow constriction; here the open flow area ranged from $S$ = 0.77 (no thermocouples) to $S$ = 0.7 (4 thermocouples). Similar work involving the synthesis of biodiesel found that the incorporation of a central rod at the centre of the baffles actually improved the mixing by suppressing channelling at the centre of the reactor [19]. Thus it can be concluded that the thermocouples do not adversely affect the reactor's mixing performance.

### 2.2 Reaction Conditions

The reaction between benzaldehyde and n-butylamine to form n-benzylidene-n-butylamine and water (Scheme 1) was used as a case study. With no solvent or thermal control, this reaction reaches a temperature of ~90 °C, higher than the boiling point of butylamine (79 °C), and has an estimated reaction enthalpy of -20 *kJ/mol* based on average bond enthalpies [20]. Therefore, high solvent ratios (20:1) are typically used to minimise the impact of the temperature rise [21]. The benzaldehyde (99%) and n-butylamine (99.5%) reagents were both supplied by Sigma Aldrich and used as supplied. Benzaldehyde was also used in the oscillation reservoir to minimise impurities. No acid catalyst was used because butylamine is a strong nucleophile. Prandtl numbers of 1:1 volumetric mixtures of benzaldehyde and n-butylamine were also calculated as $Pr$ = 19.5 and $Pr$ = 7.5 at 20 °C and 50 °C respectively.
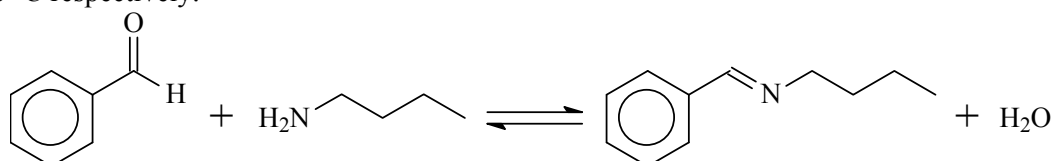


*Scheme 1 – Reaction between benzaldehyde and n-butylamine*

## 2.3 Reaction Isothermalisation

### 2.3.1 Central Composite Designs

In each of the central composite experiment designs, three factors at five factor levels were studied. The factors for the HPOBR were: net flow Reynolds number ($Re_n$); oscillatory Reynolds number ($Re_o$); and working fluid fill ratio ($FR$), defined in equations 1–3. These numbers characterise the net flow rate (residence time), oscillation intensity (plug flow and heat transfer) and heat pipe working fluid inventory (heat transfer capacity) respectively. The fill ratio shown in equation 3 is based on the entire heat pipe volume because there was no well-defined evaporator section. For the JOBR, the fill ratio was replaced with the jacket temperature. Table 1 summarises the factor levels used for each experiment set. These levels were generated using Minitab by specifying the axial star points and using $\alpha = 1.682$ to make the design rotatable.

$$Re_n = \frac{\rho v D}{\mu}$$ 
 1

$$Re_o = \frac{2\pi f x_o \rho D}{\mu}$$ 
 2

$$FR = \frac{V_{in}}{V_{hp}}$$ 
 3

In equations 1–3, $v$ is the liquid superficial velocity, $D$ is the inner diameter of the meso-OBR, $\mu$ is the liquid viscosity, $\rho$ is the liquid density, $f$ is the oscillation frequency, $x_o$ is the oscillation amplitude, $V_m$ the volume of working fluid in the heat pipe and $V_{hp}$ is the heat pipe volume.

Table 1 – Summary of the central composite experiment designs (errors based on equipment resolution)

| Run | $Re_n$ ±0.02 | $\tau$ (s) ±3 | $Re_o$ ±3 | $f$ (Hz) ±0.05 | HPOBR | | JOBR |
| | | | | | $FR$ (%) ±0.07 | $V$ (mL) ±0.05 | $T$ (°C) ±0.05 |
|---|---|---|---|---|---|---|---|
| 1 | 7.24 | 241 | 198 | 3.2 | 14.5 | 15.1 | 7.2 |
| 2 | 16.76 | 104 | 198 | 3.2 | 14.5 | 15.1 | 7.2 |
| 3 | 7.24 | 241 | 416 | 6.8 | 14.5 | 15.1 | 7.2 |
| 4 | 16.76 | 104 | 416 | 6.8 | 14.5 | 15.1 | 7.2 |
| 5 | 7.24 | 241 | 198 | 3.2 | 23.5 | 24.4 | 16.8 |
| 6 | 16.76 | 104 | 198 | 3.2 | 23.5 | 24.4 | 16.8 |
| 7 | 7.24 | 241 | 416 | 6.8 | 23.5 | 24.4 | 16.8 |
| 8 | 16.76 | 104 | 416 | 6.8 | 23.5 | 24.4 | 16.8 |
| 9 | 4 | 436 | 307 | 5 | 19.0 | 19.7 | 12 |
| 10 | 20 | 87 | 307 | 5 | 19.0 | 19.7 | 12 |
| 11 | 12 | 145 | 123 | 2 | 19.0 | 19.7 | 12 |
| 12 | 12 | 145 | 491 | 8 | 19.0 | 19.7 | 12 |
| 13 | 12 | 145 | 307 | 5 | 11.5 | 11.9 | 4 |
| 14 | 12 | 145 | 307 | 5 | 26.5 | 27.5 | 20 |
| 15 | 12 | 145 | 307 | 5 | 19.0 | 19.7 | 12 |
| 16 | 12 | 145 | 307 | 5 | 19.0 | 19.7 | 12 |
| 17 | 12 | 145 | 307 | 5 | 19.0 | 19.7 | 12 |
| 18 | 12 | 145 | 307 | 5 | 19.0 | 19.7 | 12 |
| 19 | 12 | 145 | 307 | 5 | 19.0 | 19.7 | 12 |
| 20 | 12 | 145 | 307 | 5 | 19.0 | 19.7 | 12 |

The reactions were conducted at 1:1 ratios of the benzaldehyde and n-butylamine. Both experiment sets used the same $Re_n$ and $Re_o$ ranges. $Re_n$ was changed over the range of 4–20 using the total volumetric flow rate, giving residence times of 87–436 s. $Re_n = 20$ was found in preliminary experiments to be the maximum net flow capable of being isothermalised below the boiling point of butylamine in the HPOBR. The RTD results described above were used to select $Re_n = 4$ as the lower

limit. Based on the predicted reaction enthalpy (-20 $kJ/mol$), the power output of the reaction is expected to be in the approximate range of 3–16 $W$ for corresponding net flows of $Re_n$ = 4–20.

Experiments conducted in conventional scale OBRs have shown that the oscillation frequency has a greater effect on $Nu$ than the oscillation amplitude [22]. Consequently, it was decided to use the frequency to control the oscillation intensity and thus the heat transfer rate in this study. Oscillation frequencies of 2–8 $Hz$ were chosen with an amplitude of $x_o$ = 2 $mm$, giving $Re_o$ = 123–491. This oscillation range was also based on the RTD results, and were generated using a 12.5 $mL$ syringe pump.

Appropriate heat pipe working fluids for the temperatures expected in these experiments are: water, methanol, acetone and ammonia [23]. Acetone was not compatible with the seals used in the plug valve while ammonia was rejected due to handling issues. Methanol was selected over water because it had a lower temperature limit and water would have been in the "geyser boiling" regime due to the diameter of the heat pipe annulus. A methanol fill ratio range of 11.5–26.5% was selected based on preliminary experiments. For the JOBR, jacket temperatures of 4–20 °C were chosen.

### 2.3.2 Heat Pipe Filling Procedure

With the heat pipe pressure valve open, a Cole-Palmer peristaltic pump (77521-57) fitted with Easy Load Head (77200-50) was used to transfer the desired methanol volume +1 $mL$ into the heat pipe through standard ¼" flexible tubing. Then, de-gassing (air removal) was achieved using a two-step method. First, the pressure was reduced using a KNF VP series vacuum pump (rated to 0.3 $bar$) for 30 $s$, and the heat pipe sealed by closing the pressure valve. The heat pipe was then heated using the band heater controlled with a CAL9400 temperature controller. The temperatures at three points on the surface (see Figure 1) and the heater temperature were recorded during heating using PicoLog. When the temperatures stabilised, with the vacuum pump switched on and connected to the feed line, the pressure valve was quickly opened and closed. Figure 3 shows an example of the temperatures recorded during stage 2 of the de-gassing procedure. It can be seen that after the second pressure reduction at elevated temperatures a very uniform axial temperature profile is produced.
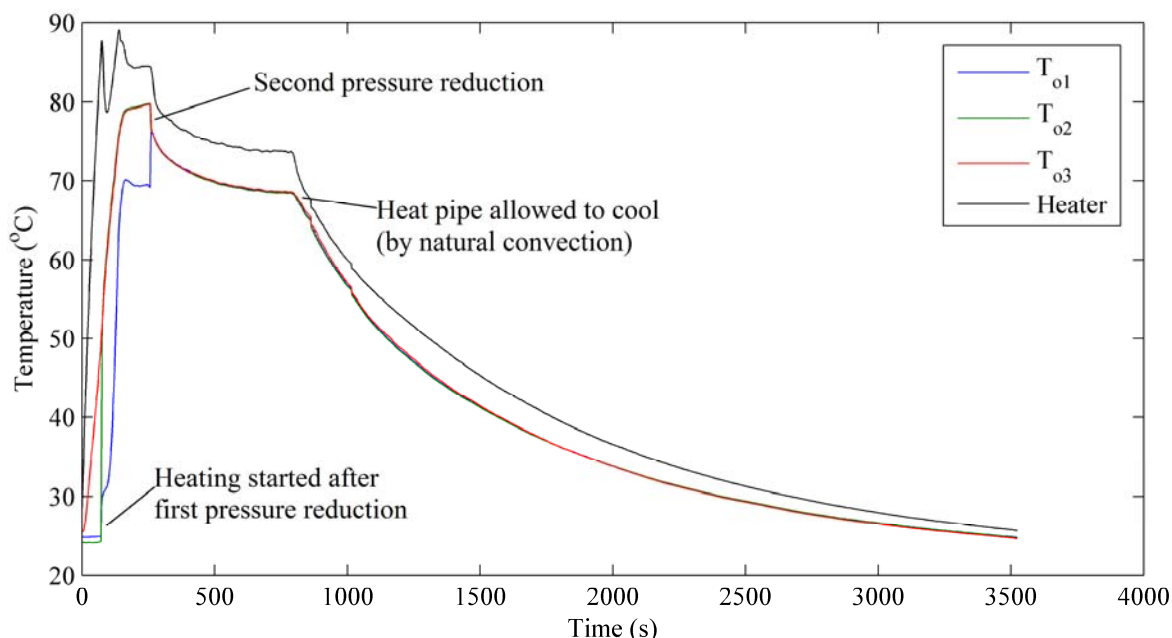


*Figure 3 – Example temperature profiles obtained during the de-gassing procedure; FR = 19% (the corresponding positions of the thermocouples is shown in Figure 1)*

### 2.3.3 Reaction Procedure

The HPOBR was positioned with the FTIR probe situated at the outlet, and the thermocouples in the arrangement shown in Figure 1. With the tubing connected to the inlet union, the reactant and oscillation lines were purged with the desired chemical. Benzaldehyde was used in the oscillation pump (with 12.5 $mL$ syringe) and one of the net flow syringe pumps (with 5 $mL$ syringe), while

7

butylamine was used in the second net flow syringe pump (with 5 *mL* syringe). The union was then connected to the reactor, and the reactor filled with benzaldehyde so that the FTIR probe tip was submerged. Next, the desired benzaldehyde net flow rate (half of the total net flow rate) and oscillation intensity were applied. Simultaneously, the FTIR recordings of the spectra and the thermocouple data logger were started. After 1 *min*, the n-butylamine net flow rate was set, initiating the reaction. Typical experiments for the HPOBR lasted ~1 *h*, until steady state was reached, after which the net flows and oscillation were stopped simultaneously with all data logging. The HPOBR was then cleaned with acetone and allowed to cool for the next experiment. Figure 4 shows a typical thermal response from the HPOBR experiments.
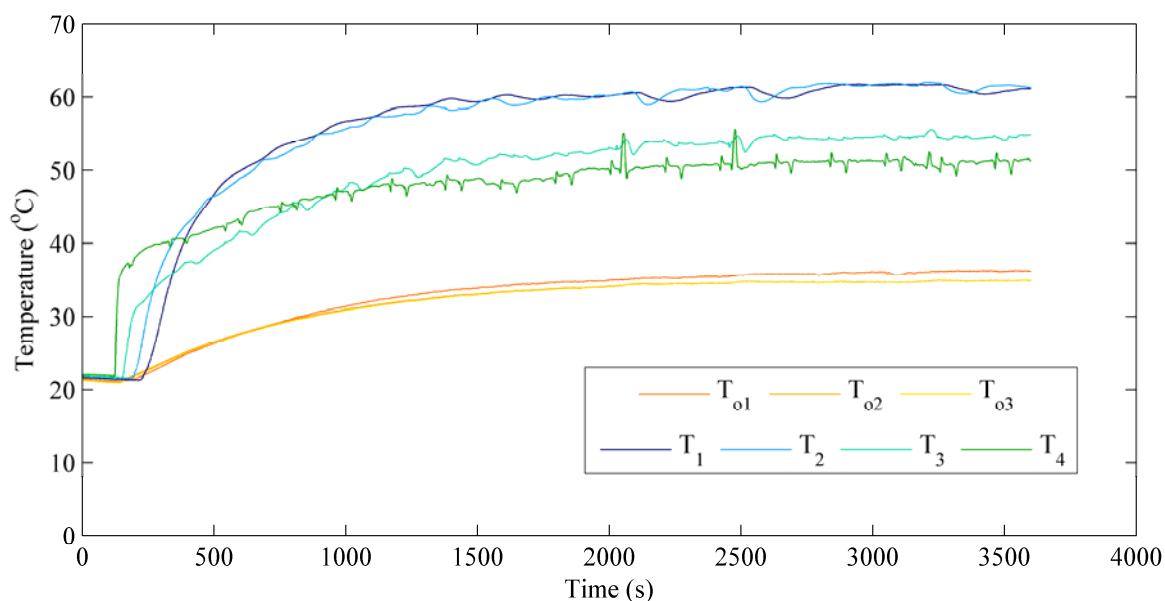


*Figure 4 – Example experiment: thermal response from the HPOBR; $Re_n$ = 12, $Re_o$ = 307, FR = 19 (the corresponding positions of the thermocouples is shown in Figure 1)*

The experiment design for the JOBR was implemented using the multi-steady state approach of previous works [21]. The JOBR was positioned with the FTIR probe at the outlet (Figure 1*b*) and the same start-up procedure as the HPOBR implemented. After steady state was reached, each of the 20 factor combinations were applied in successive 15 min intervals yielding the experiment profile shown in Figure 5. This type of experiment was possible because of the faster observed response of the JOBR, and the ability to change jacket temperature in a manner that was compatible with the screening methodology.
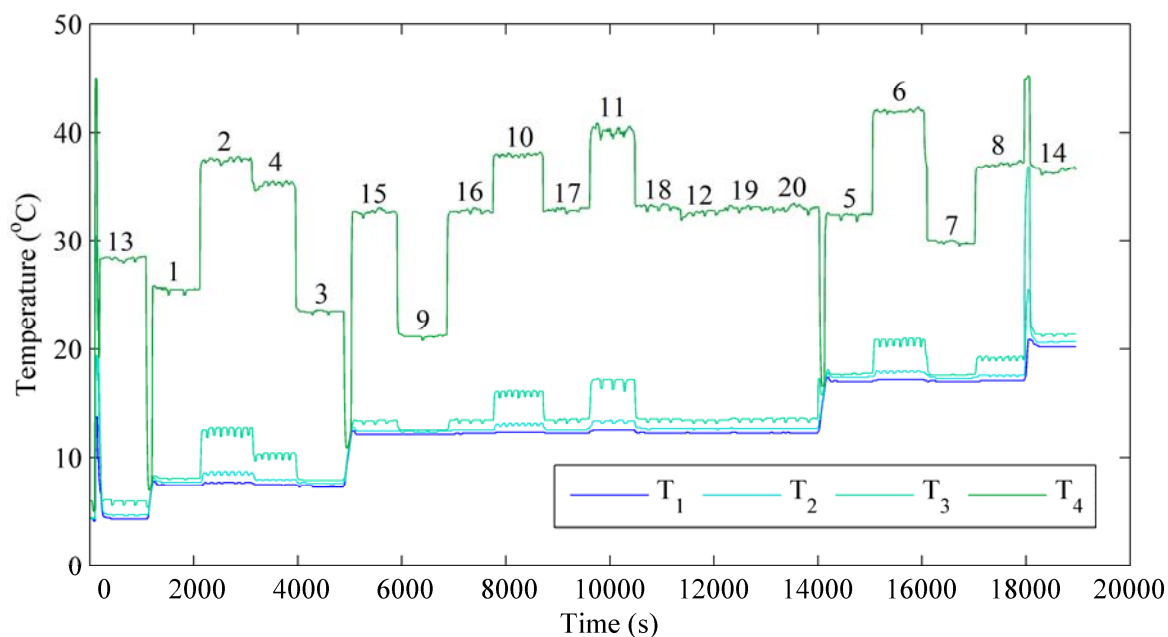
*Figure 5 – JOBR multi-steady state experiment screening profile: thermal response of the axial temperatures (the conditions corresponding to each plateau can be found in Table 1, while the equivalent positions of the thermocouples are shown in Figure 1)*

### 2.3.4 Monitoring

The main tool for characterising the reaction was Fourier Transform Infrared (FTIR) spectroscopy. The spectrometer used was a Mettler Toledo ReactIR 4000 with a mercury cadmium telluride (MCT) band detector. A DST AgX fibre conduit with 6.35 *mm* DiComp (diamond) probe was used with the HPOBR, measuring from 2000–650 $cm^{-1}$ at a resolution of 8 $cm^{-1}$ in the absorbance mode. For the JOBR experiments, a K6 conduit with 6.35 *mm* DiComp (diamond) probe was used, measuring from 4000–650 $cm^{-1}$ at a resolution of 8 $cm^{-1}$ in the absorbance mode. The FTIR was controlled using iC-IR 4.2.26 software and all spectra recorded were referenced against an air background.

In order to calibrate the imine concentration, it was first synthesised in the HPOBR. The reaction mixture collected was purified in a rotary evaporator (Buchi) at 85 *°C* with a vacuum strength of 200 *mbar* for 6 *h*. A sample of the resulting pale yellow liquid was characterised using ^{1}H-NMR with a Jeol ECS 400 NMR spectrometer. The sample was dissolved in chloroform-D and spectra recorded at 20 *°C* with a spectrometer frequency of 400 *MHz* using 16 scans with a relaxation delay of 3 *s*, and pulse width of 6.3 *s*. The ^{1}H-NMR spectrum contained the following peaks assigned to the imine: δ 8.25 (1H, s), δ 7.72 (2H, m), δ 7.40 (3H, m), δ 3.61 (2H, t), δ 1.70 (2H, q), δ 1.39 (2H, s), δ 0.94 (3H, t). The purity was estimated based on comparing the peak area at 3.61 ppm (-CH2-, imine) with a trace peak at 0.90 ppm to give 99.1%.

Analysis of the reaction profiles was achieved using principal components analysis (PCA), with the concentrations determined using partial least squares (PLS) regression. Geladi and Kowalski [24] give a good explanation of the implementation of PCA and PLS. In this study, analysis was applied in the region of 1750–1635 $cm^{-1}$, as this was found to improve the robustness of the results. Due to the presence of water as a reaction product, the reaction spectra in the region of 1750–1550 $cm^{-1}$ were deconvoluted prior to calibration. This region contained the carbonyl (~1713 $cm^{-1}$) and imine (~1652 $cm^{-1}$) peaks. In addition, second-derivatives of the spectra were taken using the 7-point Savitsky-Golay method to improve the calibration results. Calibration of the concentration was achieved by recording 5 IR spectra using a 15 *s* scan time on various samples of benzaldehyde and the imine product at different volume ratios. The calibration data was split into 56 training samples, and 18 validation samples.

9

# 3 Results and Discussions

## 3.1 HPOBR

### 3.1.1 Reaction Temperature Profile: Main Effects

Figure 6 shows the main effects plots for the steady-state responses of the thermocouples obtained for the HPOBR. These plots were created by taking the average of the data points across the three factor planes in the design space. For example, the average of $Re_n$ = 7.24 was made at two $Re_o$ levels (198 and 416) and $FR$ levels (14.54 and 23.46). Thus, the ratios of error magnitude to correlation are analogous to the statistical significance of the factor. The four sets of plots refer to the temperatures recorded by thermocouples $T_1$ to $T_4$, from the top of the reactor to the base respectively.

It was observed that larger reactant net flow rates produced higher operating temperatures, an expected result of increased chemical potential energy supply to the reactor. Thermocouples $T_1$ and $T_2$ (closest to the outlet) measured more linear responses to the increase in $Re_n$, whilst thermocouples $T_3$ and $T_4$ showed temperature maxima around $Re_n$ = 18. This is likely to be a consequence of shifting the position of the maximum in reaction exotherm downstream.
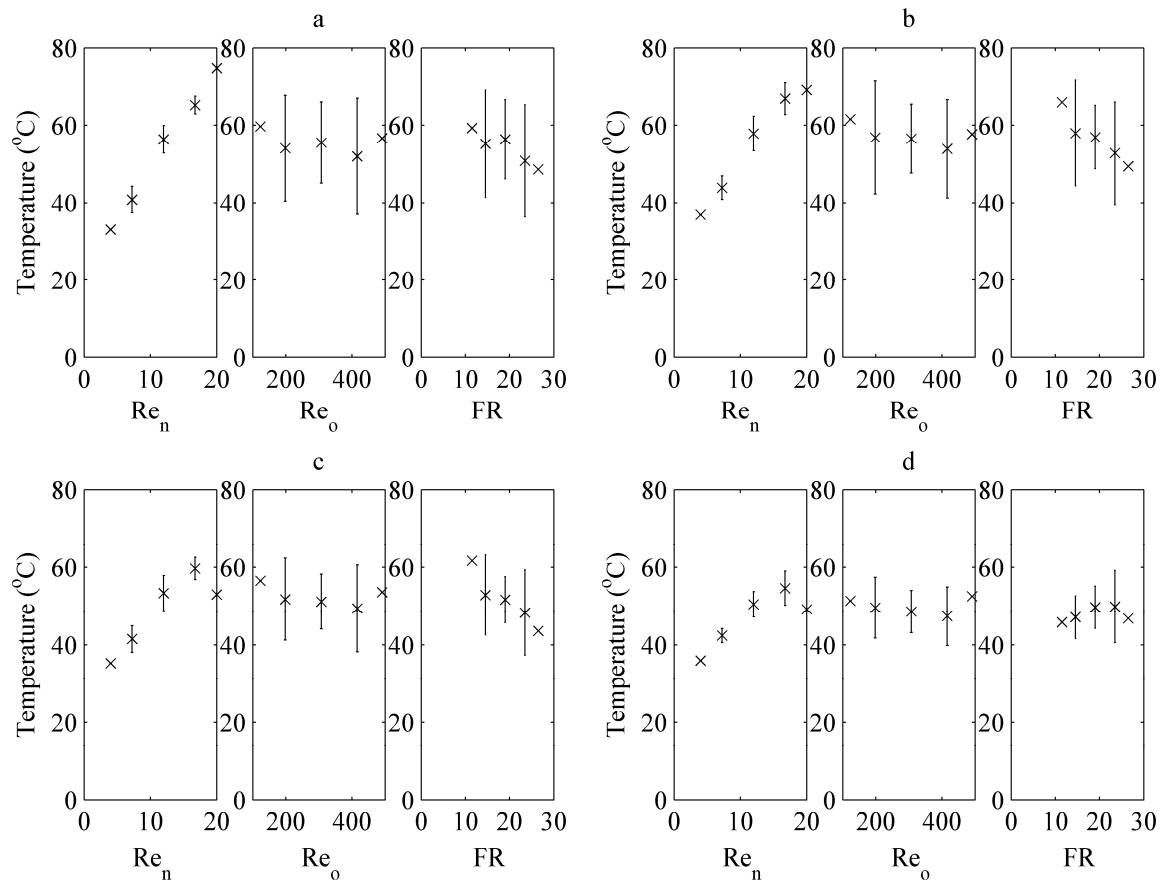


*Figure 6 – Main effects plots for the steady-state reaction temperatures measured in the HPOBR; (a) $T_1$, (b) $T_2$, (c) $T_3$, (d) $T_4$ (see Figure 1 for corresponding thermocouple locations)*

It has been shown experimentally that up to 30-fold improvements in tube-side Nusselt number can be realised in shell-and-tube heat exchangers when the tube-side fluid is oscillated in the presence of baffles [22]. More recently, it has been shown that up to 4-fold increases in $Nu$ can be obtained in mesoscale OBRs fitted with helical baffles when increasing the oscillation intensity from $Re_o$ = 100–320 [18]. The heat transfer enhancement is believed to be a consequence of increased radial motion, leading to higher exposure of the bulk liquid to the surface. In Figure 6 it can be seen that the operating temperature does decrease by a small amount when increasing the oscillation intensity. However, the observed trends are minor, with a high degree of scatter and large error magnitude observed suggesting no statistical significance. This apparent non-significance could be because the rate-limiting step for heat transfer is on the shell-side (i.e. in the heat pipe). This is justified based on

the JOBR results discussed later; in the JOBR the effect of $Re_o$ was found to be significant for the inlet temperature $T_1$, even with a thicker glass wall used.

Thermosyphons have a number of operating limits that could account for a rate-limiting step at a particular power input. For example, the viscous limit describes the tendency of the vapour flow to become hindered if the vapour pressure drop reaches a similar magnitude to the vapour pressure within the evaporator [25]. Similarly, the sonic limit occurs when the vapour flow reaches sonic speeds and becomes choked. In both cases the heat transfer rate is limited. However, these are not likely to explain the results observed in HPOBR, particularly because the predicted power inputs for this reaction were low (up to 16 $W$) and the average operating temperatures observed were within the usable temperature range of the methanol working fluid (10–150 °C) [23]. Alternative explanations include partial dry-out of the working fluid, entrainment and liquid film maldistribution. For dry-out, or partial dry-out, the heat transfer rate in the evaporator region would be limited by the thermal capacity of the remaining liquid film on the meso-OBR wall. Similarly, maldistribution of the film around the meso-OBR tube in the condenser region would limit the amount of energy transferred back to the reaction. Entrainment (flooding) of the working fluid in the vapour can also hinder the flow of the liquid film [26]. Therefore, future work should address the working fluid selection and operation in more detail.

The final factor studied was heat pipe fill ratio. It was observed that increased working fluid volumes caused the temperatures measured by thermocouples $T_1$–$T_3$ to decrease. Because there was no significant trend observed of the $FR$ on the response measured by thermocouple $T_4$, the net effect of increasing $FR$ was a more uniform axial temperature profile of the reaction mixture.

In two-phase thermosyphons there is an optimum liquid volume to generate the maximum heat transfer rate. Insufficient working fluid volumes lead to dry-out whilst larger volumes risk liquid entrainment in the vapour [26]. Han and Cho observed this experimentally [27]. If the dry-out regime was approached in the HPOBR at the low working fluid volume level, then the reaction would be insufficiently cooled. The expectation is a higher operating temperature downstream, which is indeed observed in the results presented in Figure 6. Therefore, it can be concluded that for the design space employed in this study, the HPOBR is more effective at higher working fluid inventories.

*3.1.2 Regression Models for the Reaction Temperature*

To better visualise the thermal response of the HPOBR, regression models were fitted to each of the thermocouple responses measuring the axial temperature profile of the reaction. In all cases, it was possible to simplify the regression model to a set of linear and parabolic terms through stepwise regression using a significance level of 0.05. The models were chosen to maintain hierarchy, and a good fit was produced in each case. The final regression models obtained are shown in equations 4–7. Each model is only applicable to the design space used in this study. These regression models had respective adjusted $R^2$ values of 93.72%, 95.09%, 88.35% and 68.88%. Additionally, each model produced normally distributed residuals and no underlying structures were present in the residuals vs fits plots, indicating no unaccounted factor effects. The low adjusted $R^2$ value for $T_4$ is a result of simplifying the regression model to improve robustness.

$$T_1 = 34.88 + 2.583\, Re_n - 0.585\, FR \qquad\qquad 4$$

$$T_2 = 37.62 + 4.232\, Re_n - 0.01222\, Re_o - 0.796\, FR - 0.0826\, Re_n^2 \qquad\qquad 5$$

$$T_3 = 29.59 + 4.94\, Re_n - 0.801\, FR - 0.14\, Re_n^2 \qquad\qquad 6$$

$$T_4 = 20.67 + 3.911\, Re_n - 0.1173\, Re_n^2 \qquad\qquad 7$$

The regression models obtained largely reflect the observations of the main effects in Figure 6. For the inlet temperature (equation 7) only the net flow was statistically significant, producing a parabolic correlation. The fill ratio did not affect the inlet temperature because this point was likely always submerged within the working fluid. For thermocouples $T_2$ and $T_3$ (equations 5 and 6 respectively), the parabolic effect of $Re_n$ is captured along with the negative correlation with $FR$. As mentioned, this parabolic behaviour was a result of shifting the reaction exotherm downstream. Interestingly $Re_o$ was also negatively correlated with the response measured from thermocouple $T_2$, whereas it appeared to be statistically insignificant in the main effects plot. The statistical importance of $Re_o$ in the regression model for thermocouple $T_2$ could be the result of maldistribution of the

11

working fluid film, or may simply be an artefact of the increased scatter in the results. Finally, the effects of net flow rate and fill ratio have been captured for thermocouple $T_1$ (equation 4). In all regression models obtained, no two-way interactions were required.

*3.1.3 Reaction Isothermalisation Performance*

Figure 7a shows the average operating temperature plotted at different isosurfaces in the design space used in this study. This plot was obtained by averaging the four regression models in equations 4–7). As shown in the main effects plots, the oscillation intensity was not statistically significant for thermocouples $T_1$, $T_3$ and $T_4$. This is reflected by the operating temperature's invariance to the oscillation intensity; i.e. the isosurfaces are parallel with the $Re_o$ axis. The net flow ($Re_n$) has the most dominant effect in the tested range, with higher average operating temperatures produced at larger $Re_n$. Finally, the fill ratio is negatively correlated with the operating temperature suggesting that the cooling capacity is greater for larger working fluid volumes The steeper isosurface gradient at higher $Re_n$ indicates that there is a slight interaction between the net flow rate and working fluid volume. Here it is observed that increased working fluid inventory is required to lower the operating temperature at higher reactant flow rates because of the increased chemical potential energy supplied to the HPOBR.
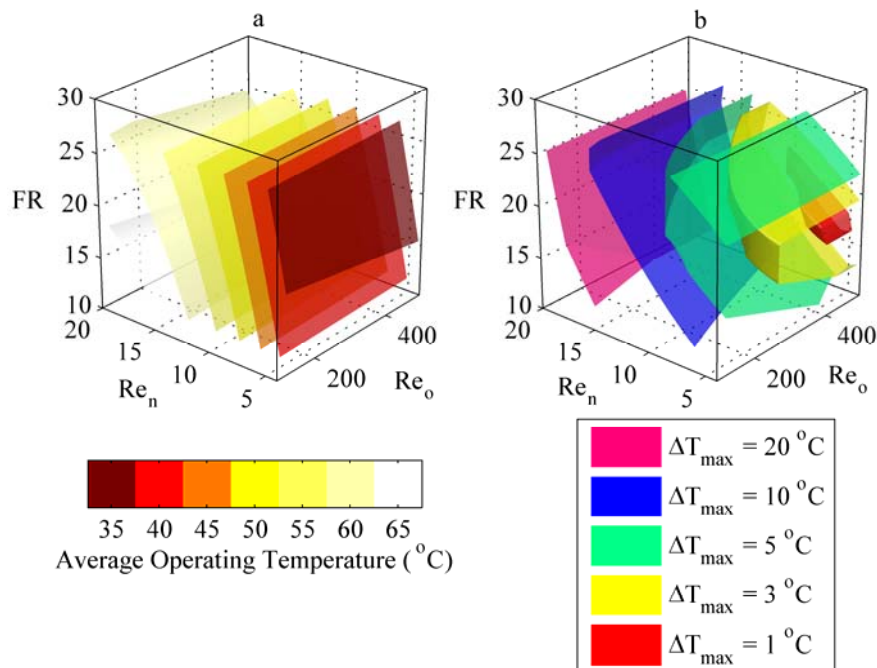


*Figure 7 – 3D response maps of reaction thermocouple regression models from the HPOBR experiments; (a) average steady-state temperature, (b) contours of isothermal operation*

In all 20 experiments, the temperatures recorded did not exceed the boiling point of butylamine, indicating successful thermal management. However, in some experiments a large axial temperature difference was still observed. Therefore, in addition to calculating the average operating temperature it was also possible using the regression models to locate where in the design space isothermal operation was expected to occur. Figure 7b shows five such isosurfaces of maximum temperature spread. These were defined by taking the maximum temperature difference between the four thermocouple readings at each point in the design space. The red and yellow contours represent satisfactory isothermal performance, with maximum spreads of 1 °C and 3 °C respectively. The 1 °C temperature spread occurs within the region of $Re_n$ = 5–11, $Re_o$ > 400, $FR$ = 16–23. Surprisingly, although $Re_o$ showed no statistical significance for $T_1$, $T_3$ and $T_4$ (and the average operating temperature), its statistical significance for $T_2$ means the oscillation intensity does impact upon the degree of isothermalisation. Additionally, for an isothermal flow to be produced, the fill ratio must be chosen for the particular $Re_n$ in the range of $Re_n$ = 5–11, demonstrating an interaction between these parameters not observed directly in the regression models.

12

*3.1.4 Heat Pipe External Surface Temperature*

The thermal responses measured using the thermocouples fitted to the outer edge of the HPOBR were treated with the same analysis as the thermocouples measuring the reaction mixture temperature. The main effects were mostly similar, with the net flow having the dominating effect. The lower and middle thermocouple responses were also negatively correlated with the fill ratio, and a two-way interaction between $Re_n$ and $FR$ was present. Here, increasing the fill ratio was more significant at higher net flow rate, with higher temperatures produced at larger working fluid volumes.

The regression models for the thermal responses measured from the top, middle and bottom of the outer HPOBR surface are shown in equations 8–10, with adjusted $R^2$ values of 96.4%, 85.1% and 81.6% respectively. These models presented normally distributed residuals. No underlying structures were detected in the residuals vs fits plots.

$$T_{e1} = 23.887 + 1.0361\,Re_n \qquad\qquad 8$$

$$T_{e2} = 30.79 + 0.86\,Re_n - 0.566\,FR - 0.0524\,Re_n^2 + 0.0586\,Re_n FR \qquad\qquad 9$$

$$T_{e3} = 28.67 + 0.677\,Re_n - 0.422\,FR - 0.0493\,Re_n^2 + 0.00657\,Re_n FR \qquad\qquad 10$$

Figure 8a shows the average temperature difference between the reaction mixture and external surface; i.e. the difference between the average temperature predicted by equations 8–10 and the average temperature predicted by equations 4–7. It can be seen that the smallest difference occurred at the lowest net flow rate and highest working fluid volume and higher oscillation intensities. In contrast, the largest temperature difference occurred at the highest net flow rates and lowest fill ratios. The external surface temperature overall varied between 27.8 *°C* and 43.4 *°C* depending on the operating conditions applied; a 15.6 *°C* difference. Figure 8b shows the isothermal behaviour of the outer HPOBR surface. It is observed that for the majority of the design space explored, the external surface exhibited a uniform temperature in contrast to the reaction itself.

It can be inferred from these results that the HPOBR functions primarily through energy spreading, because the heat removal rate from the external surface via natural convection increases at a slower rate than the increase in reaction temperature when increasing the reactant net flow rate.
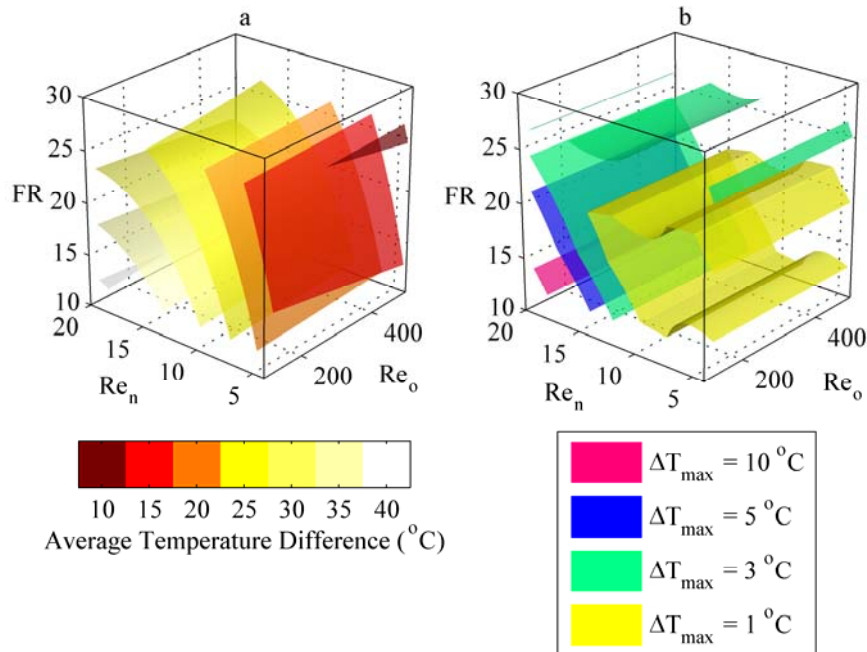


*Figure 8 – 3D response maps of the external thermocouple regression models from the HPOBR experiments; (a) difference in temperature between the reaction mixture and external surface, (b) contours of isothermal operation of the external surface*

13

*3.1.5 Chemical Response*

The imination reaction under investigation here typically uses a high solvent excess (20:1) to avoid excessive heat release during the reaction [21]. In removing this solvent, the processing volume is reduced by a factor of 20. For process intensification, this means the reactor volume can also be reduced by the same margin to achieve the same throughput. Further, it was found that removing the large dilution otherwise created by the solvent, in combination with the elevated operating temperatures, caused the reaction rate to be approximately 13 times faster than the reaction when conducted at 0.25 *M* concentrations [21] (these data are not shown here). Therefore, the solventless synthesis of this imination reaction in the HPOBR provides a combined 260-fold intensification compared with the reaction performed in solvent whilst improving the conversion.

Another benefit of removing the solvent was the equilibrium was shifted towards the product. In 17 of the 20 experiments performed in the HPOBR, the reaction conversion reached 100%, making the fitting of regression models to these results redundant. The time for the reaction to reach steady state was independent of the operating conditions, and varied between 1000–3000 *s*. This high conversion was a consequence of reduced dilution, and high operating temperatures. Instead, Principal Components Analysis (PCA) was performed in order to compare the two reactor configurations. Figure 9 shows the bivariate scores plot of the first two principal components describing the FTIR spectra in the HPOBR.

Water is a product of the imination reaction and was found to be immiscible with the benzaldehyde reactant and imine product. Depending on the mixing intensity, the water would either form a well-mixed emulsion phase or exit the reactor in slugs. Therefore, the effect of water was removed by taking the 2$^{nd}$ derivative of the reaction spectra. It can be seen that only experiment runs 7, 8, 10 and 14 can be reliably differentiated. These experiment runs corresponded to conditions with higher fill ratios (higher heat spreading capacity) or higher net flow rate (lower residence time) where the conversion did not reach 100%. Thus, chemical variation can be differentiated in the HPOBR.
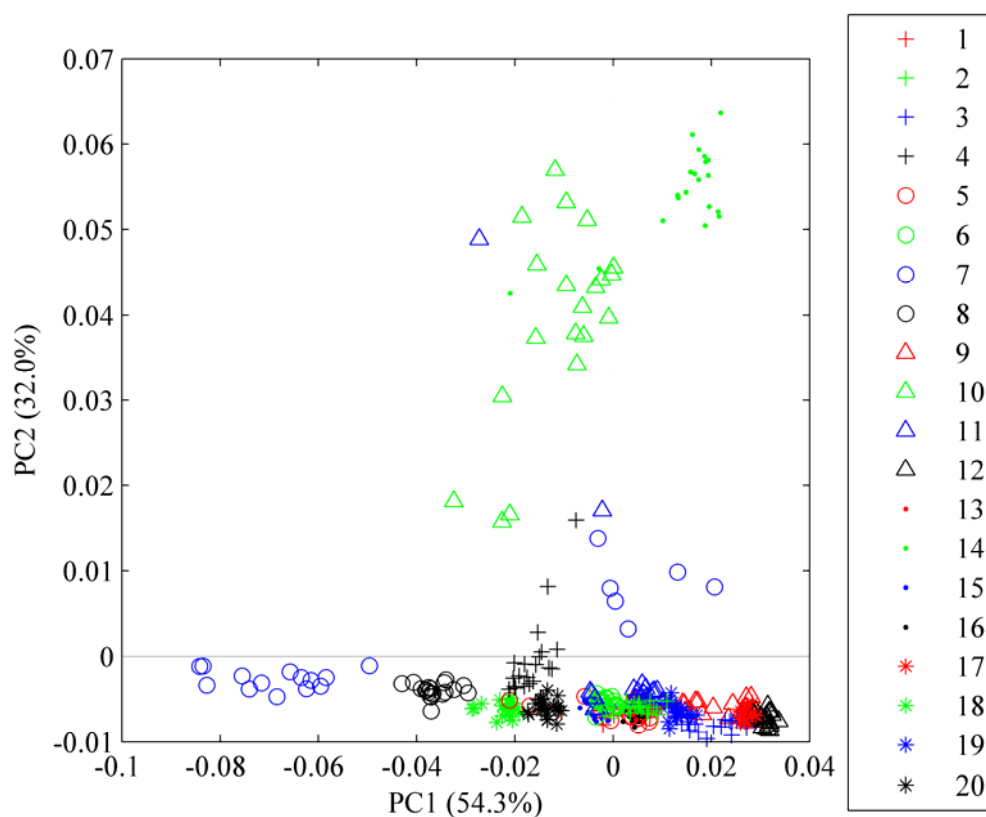


*Figure 9 – Bivariate scores plot after 2$^{nd}$ derivative treatment for the steady-state HPOBR FTIR data; legend entries refer to the operating parameter combinations summarised in Table 1*

## 3.2 JOBR

### 3.2.1 Reaction Temperature Profile: Main Effects

Figure 10 shows the main effects for the steady-state operating temperatures in the JOBR. Firstly, unlike the HPOBR results, only the inlet temperature (thermocouple $T_4$) was significantly affected by $Re_n$. Here a similar trend to the HPOBR was observed, with a maximum produced around $Re_n = 17$. Thermocouple $T_3$ measured a slight linear correlation between $Re_n$ and the temperature, but the overall effect was less significant, as shown by the magnitude of the errors. The main reason for the difference in performance between the two reactors is the mechanism in which heat transfer occurs. The HPOBR primarily functions through energy spreading, with some heat release to the surroundings based on natural convection. In contrast, the JOBR only possesses the energy removal capability.

Increasing $Re_o$ was observed to decrease the temperature measured at positions $T_3$ and $T_4$. The inlet thermocouple was more significantly affected, with the slope levelling around $Re_o = 416$. This is in direct contrast to the HPOBR, which showed no statistical significance of the oscillation intensity. Here, it is likely that for low oscillation intensities the rate-limiting step for heat transfer falls on the tube-side.

Finally, all measured axial temperatures increased linearly with an increase in the jacket temperature as would be expected. The inlet temperature was found to be larger than the downstream temperatures because of the increased reaction rate in this section. The temperature recorded by thermocouple $T_3$ was found to be slightly larger than the jacket temperature, and the two temperatures measured closer to the outlet ($T_2$ and $T_1$) were found to reach the jacket temperature. Generally the temperatures measured in the JOBR were lower than the HPOBR. Again, this is because of the differing mechanisms for heat transfer and the larger thermal mass of the jacket.
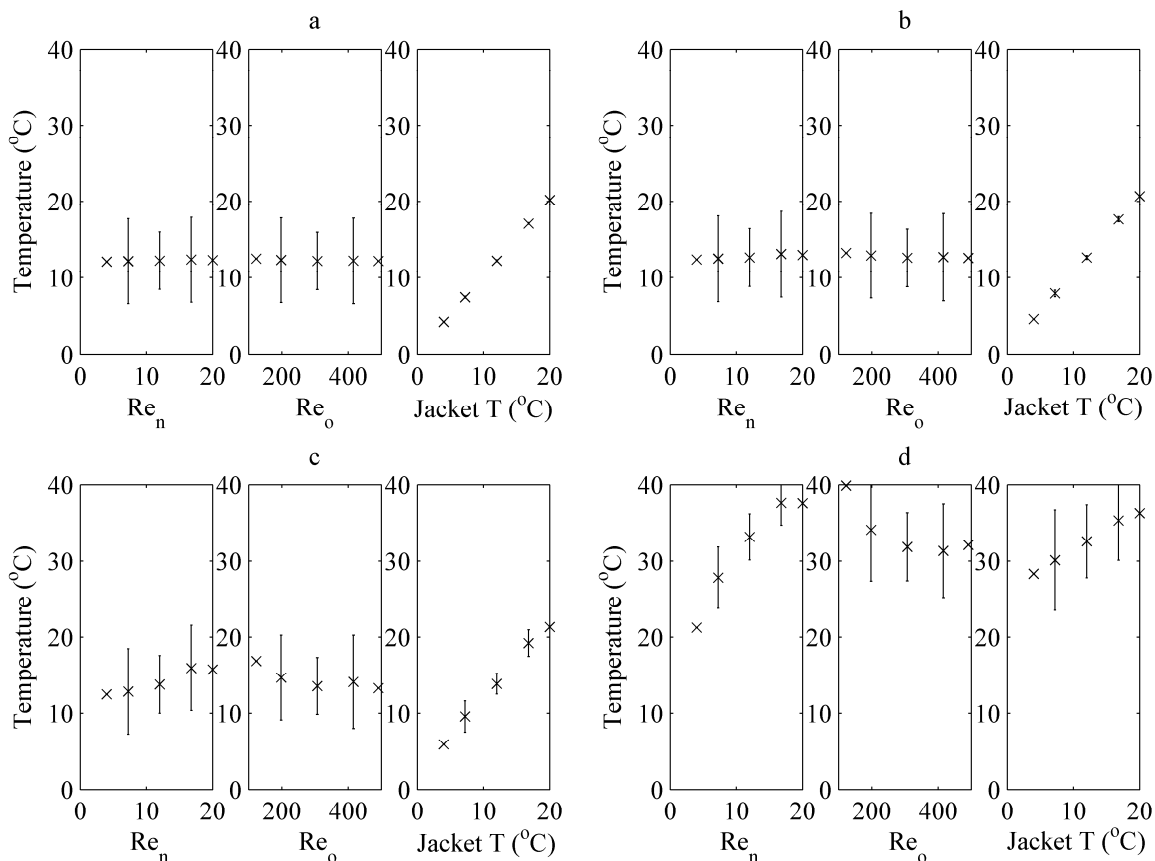


Figure 10 – Main effects plots for the steady-state reaction temperatures measured in the JOBR; (a) $T_1$, (b) $T_2$, (c) $T_3$, (d) $T_4$ (see Figure 1 for corresponding thermocouple locations)

*3.2.2 Regression Models for the Reaction Temperature*

      Each of the four measured axial temperature responses from the JOBR experiments were again treated to statistical analysis. The regression models obtained are summarised in equations 11–14. The respective adjusted $R^2$ values for each regression model were 99.91%, 99.70%, 97.64% and 97.95%. Additionally, the residuals were normally distributed and no structure was observed in the residuals vs fits plots. These regression models largely reflect the observations of the main effects plots. The linear and parabolic effects of $Re_n$ and $Re_o$, and the linear effect of the jacket temperature are captured for the inlet temperature ($T_4$). For each subsequent response moving towards the outlet, the effects of $Re_n$ and $Re_o$ diminish until only the jacket temperature affects the reaction temperature at the outlet ($T_1$). It must be noted that these models apply only for the design space tested.

$$T_1 = 0.1923 + 1.00451\,T \tag{11}$$

$$T_2 = -0.059 + 0.0512\,Re_n + 1.0128\,T \tag{12}$$

$$T_3 = 4.76 + 0.2756\,Re_n - 0.03552\,Re_o + 0.992\,T + 0.000049\,Re_o^2 \tag{13}$$

$$T_4 = 22.01 + 2.15\,Re_n - 0.0811\,Re_o + 0.5277\,T - 0.04681\,Re_n^2 + 0.000106\,Re_o^2 \tag{14}$$

*3.2.3 Isothermalisation Performance*

      Figure 11a shows isosurfaces of the inlet temperature plotted using equations 11–14 within the experiment design space, providing an overview of the temperature response of the reaction. The net flow rate is observed to have the most significant effect, with higher temperatures produced at larger values of $Re_n$. Lower jacket temperatures are shown to lower the inlet temperature. This can be seen by the gradient of the isosurfaces in this plane. Finally, the effect of $Re_o$ is observable in contrast to the HPOBR results, with the isosurfaces curved in the $Re_o$ axis. Increasing the oscillation intensity at constant $Re_n$ and jacket temperature results in decreased temperature (i.e. moving to a new isosurface). Here, an optimum around $Re_o = 416$ is apparent, especially at low jacket temperature and high net flow rate, which was not observed in the main effects plot. This optimum may exist because there is a trade-off between increased heat transfer rate and increased reaction heat release due to increased mixing.

      The regression models obtained in the JOBR were used to visualise the isothermal performance of the reactor. Figure 11b shows isosurfaces of maximum temperature spread measured between the four axial thermocouples within the reactor. Here, a much larger minimum temperature spread of 7.5 °C was produced, corresponding to low net flow, high jacket temperature and optimal mixing. Based on this result, it appears that only an approximation to isothermal operation can be achieved, representing a 'brute-force' approach. This is problematic from a reactor point of view because it limits the throughput at which desirable isothermal behaviour is achieved. In this regard, the HPOBR appears to be superior. This is particularly attractive allied to its passive operation, meaning that no other devices are required, e.g. to supply cooling fluid.

      However, the JOBR has advantages over the HPOBR. Principally, the larger thermal mass of the jacket means higher throughputs can be obtained, albeit at the expense of large temperature disparities. Another advantage of the JOBR is greater flexibility. In the HPOBR with this imination reaction $Re_n = 20$ was found to be the largest that could be implemented to ensure the temperature did not exceed the boiling point of the butylamine reactant (79 °C). This may be because the reaction exotherm energy was not sufficiently captured by the working fluid. However, simply increasing the working fluid volume is not sufficient to improve the cooling response because it decreases the usable lengths of the adiabatic and condenser sections. The current HPOBR is therefore applicable over a narrower operating window. Potential methods to increase the usable operating window are: (1) longer reactor length/larger heat pipe annulus diameter (allowing for larger working fluid volume), and (2) the use of a wick to improve working fluid distribution. Alternatively, a liquid with higher latent heat such as water could be used (although the change in usable temperature range must be taken into account). The final advantage of the JOBR was a quicker response time (as observed in the multi-steady state temperature profiles in Figure 5).
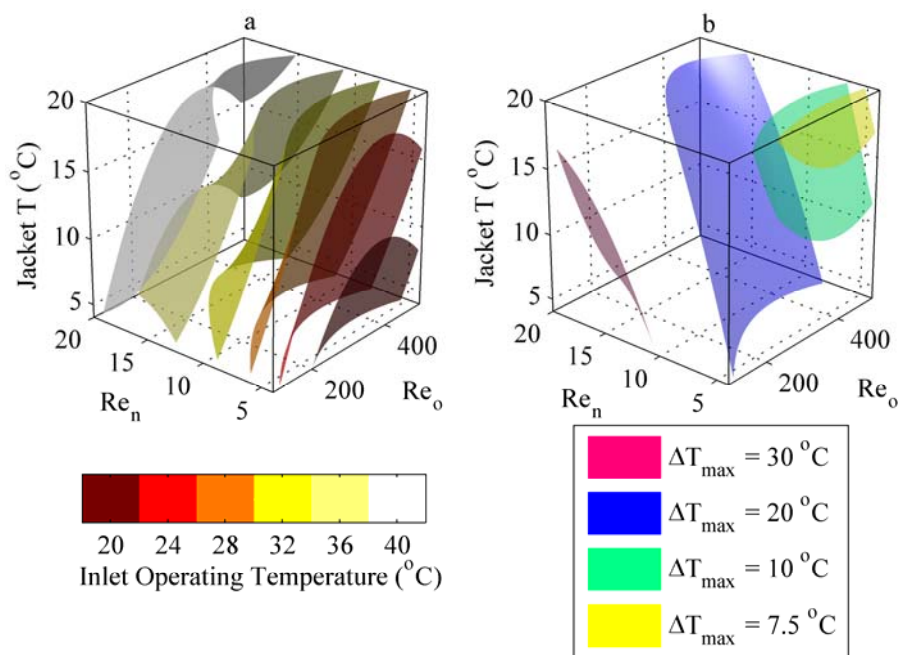
*Figure 11 – 3D response maps of thermocouple regression models from the JOBR experiments; (a) inlet steady-state temperature, (b) contours of isothermal operation*

### 3.2.4 Chemical Response

In the JOBR, although the same residence times as the HPOBR were used, the reaction did not reach completion because the operating temperatures attained were lower than in the HPOBR as a consequence of the larger thermal mass of the cooling jacket. Therefore, the reaction conversion was determined using equation 15. Here, $F_b$ is the number of moles of benzaldehyde at the reactor outlet, and $F_{b,0}$ is the number of moles of benzaldehyde entering the reactor. The concentration at the outlet was determined by comparing the measured reaction spectra obtained in the experiment with calibration spectra using partial least squares regression. The number of moles was determined by multiplying the concentration by the volumetric flow rate.

$$X = \frac{F_{b,0} - F_b}{F_{b,0}}$$
15

Figure 12 summarises the main effects plots of the reaction conversion. It was found that the conversion was largely consistent over the factor space explored. Only the net flow rate had a significant impact, with larger residence times (lower $Re_n$) producing higher conversions.

The final insights of the chemical response were made using principal components analysis (PCA), which has the benefit of analysing all recorded FTIR data simultaneously. Figure 13 shows the scores vs scores plot for the first three principal components, describing a total of 96.4% of the variation in the FTIR spectra. In comparison to the HPOBR data, the steady-state clusters are better segregated allowing for better distinction of the effect of each factor level combination. It can be seen that the points corresponding to runs 15–20 (experiment centre points) also overlap as expected.

It was found that the structure of the principal components aligned with the benzaldehyde and imine spectra, suggesting that the sample clusters observed in Figure 13 are a result of chemical variation and not differing amounts of water around the FTIR probe. This result shows that there is a potential for screening the kinetics of solventless exothermic reactions in addition to optimisation. The benefits of reduced solvent consumption in this regard are intensified reaction rate from reduced dilution and minimisation of downstream purification. The intensified reaction rate also enables secondary advantages. These include reduced reactor volume requirements to deliver a particular throughput, or the ability to deliver much greater throughputs for the same reactor volume. The latter would enable scale-up to be realised without the need for re-optimisation after screening.
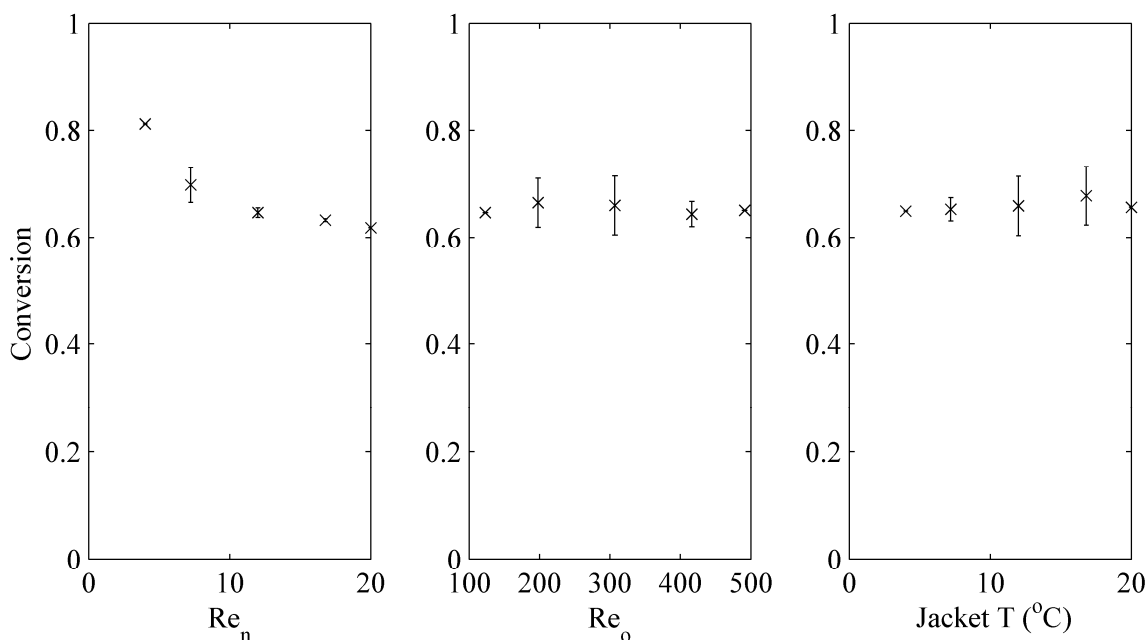
17

*Figure 12 – Main effects plots of the reaction conversion for the JOBR experiments*
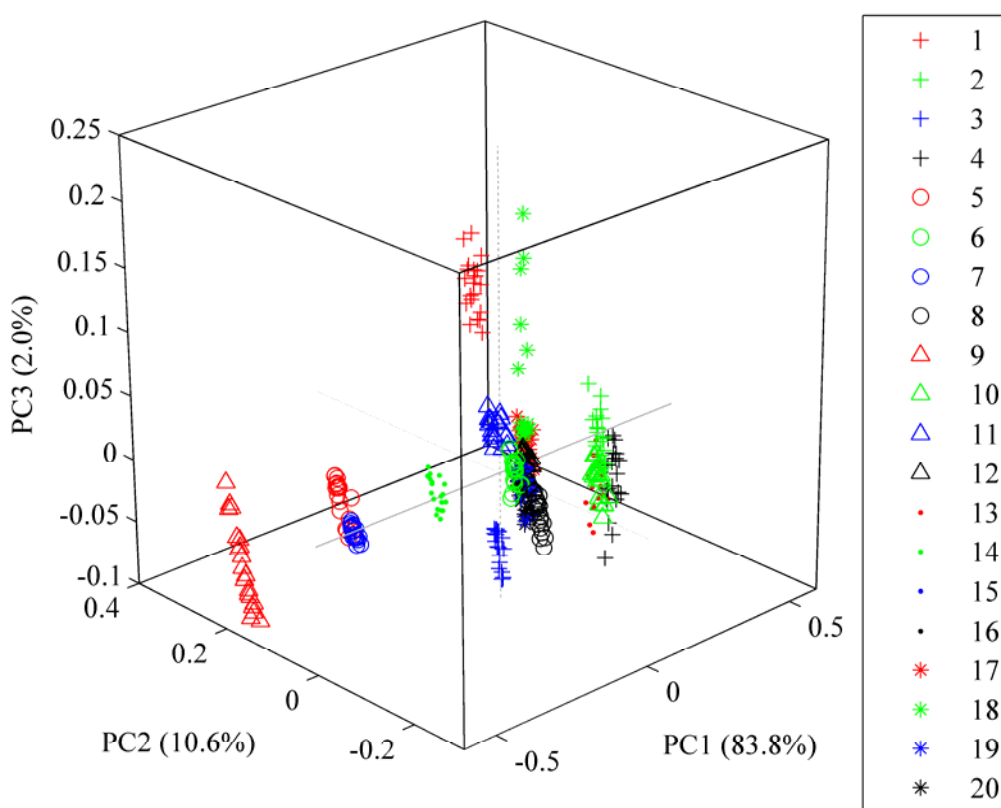


*Figure 13 – Trivariate scores plot for the steady-state JOBR FTIR data; legend entries refer to the operating parameter combinations summarised in Table 1*

## 4 Conclusions

A new "heat pipe oscillatory baffled reactor" (HPOBR) was developed and compared to a conventional jacketed oscillatory baffled reactor for the thermal control of an exothermic imination reaction between benzaldehyde and butylamine, operating in the absence of solvent.

Central composite experiment designs were used to explore the effects of reactant net flow rate (residence time), fluid oscillation intensity and cooling capacity by controlling the following

respective dimensionless groups: $Re_n$, $Re_o$ and $FR$. In the jacketed oscillatory baffled reactor (JOBR), the fill ratio was replaced with jacket temperature.

The main findings and operational differences between the two reaction platforms are summarised below:

- The HPOBR was able to prevent the reaction from exceeding the boiling point of the butylamine reactant at all conditions tested, and also demonstrated the capacity for achieving isothermal behaviour (thermal steady state reached in 1200–2400 $s$ depending on the operating conditions). The key advantage over the jacketed OBR was that a constant supply of coolant was not required: the HPOBR operated "passively", and functioned as an energy spreader rather than a heat sink.

- The reaction conversion reached 100% in the HPOBR in 17 of the 20 experiments (with steady state reached after 1000–3000 $s$ depending on the operating conditions). The incomplete reactions corresponded to experiment conditions with high fill ratios and low residence times. Subsequent analysis of the FTIR data using PCA showed that chemical variation as a result of reaction incompletion can be distinguished.

- The JOBR was able to produce lower operating temperatures than the HPOBR because of the larger thermal mass of the jacket. Consequently, the reaction conversion was lower with the optimal conversion occurring at high residence time (low $Re_n$). Analysis of the JOBR FTIR spectra using PCA showed that the different steady-state spectra could again be distinguished easily as a consequence of chemical variation, offering the potential to screen the kinetics of solventless exothermic reactions at milli-fluidic scales in the future.

- Another benefit of the JOBR was greater flexibility, offering the potential to use a wider flow rate range. However, the main disadvantage of the JOBR was that isothermal behaviour could not be realised within the design space explored. Therefore it would be difficult to use the JOBR as a flow chemistry platform if temperature were a screening variable. The HPOBR in principle offers a flow chemistry platform in which "temperature screening" is more readily achievable, which would allow rapid determination of e.g. activation energies and pre-exponential factors for Arrhenius rate expressions.

- The HPOBR has exhibited a 20-fold reduction in processing volume because of the removal of the solvent, and an additional 13-fold improvement in reaction rate as a result of reduced dilution and high operating temperature compared with the reaction performed in a solvent. A reactor based on this design would be 260 times smaller than a reactor using conventional conditions.

**Nomenclature**

| | |
|---|---|
| $D$ | Tube diameter ($m$) |
| $f$ | Fluid oscillation frequency ($Hz$) |
| $F_b$ | Outlet number of moles of benzaldehyde ($mol$) |
| $F_{b,0}$ | Inlet number of moles of benzaldehyde ($mol$) |
| $FR$ | Heat pipe fill ratio ($=V_m/V_{hp}$) |
| $Ma$ | Mach number of the working fluid |
| $N$ | Number of equivalent tanks-in-series |
| $Re_n$ | Net flow Reynolds number ($=\rho v D/\mu$) |
| $Re_o$ | Oscillatory Reynolds number ($=2\pi f x_o \rho D/\mu$) |
| $T_i$ | Temperature measured at position $i$ |
| $V_{hp}$ | Working volume of heat pipe ($mL$) |

19

$V_m$      Volume of working fluid in heat pipe ($mL$)
$x_o$      Fluid oscillation amplitude ($m$)
$X$        Reaction conversion

*Greek Letters*
$\mu$      Liquid viscosity ($Pa.s$)
$\rho$     Liquid density ($kg/m^3$)

**References**

[1]     D. Reay and A. Harvey, The role of heat pipes in intensified unit operations, Applied Thermal Engineering 57 (2013) 147-153

[2]     J.R. McDonough, A.N. Phan, and A.P. Harvey, Rapid process development using oscillatory baffled mesoreactors - A state-of-the-art review, Chemical Engineering Journal 265 (2015) 110-121

[3]     H. Löwe, R. Axinte, D. Breuch, and C. Hofmann, Heat pipe controlled syntheses of ionic liquids in microstructured reactors, Chem. Eng. J. 155 (2009) 548-550

[4]     S. Wong, H. Hsiao, and K. Lo, Improving temperature uniformity and performance of CO preferential oxidation for hydrogen-rich reformate with a heat pipe, Int. J. Hydrogen Energy 39 (2014) 6492-6496

[5]     J.M. Leimart, P. Treiber, and J. Karl, The Heatpipe Reformer with optimized combustor design for enhanced cold gas efficiency, Fuel Processing Technology 141 (2016) 68-73

[6]     A.F. Abdel-Magid, K.G. Carson, B.D. Haris, C.A. Maryanoff, and R.D. Shah, Reductive Amination of Aldehyde and Ketones with Sodium Triacetoxyborohydride. Studies on Direct and Indirect Reductive Amination Procedures, J. Org. Chem. 61 (1996) 3849-3862

[7]     V.I. Tararov, R. Kadyrov, T.H. Riermeier, C. Fischer, and A. Borner, Direct Reductive Amination versus Hydrogenation of Intermediates - A Comparison, Adv. Synth. Catal. 346 (2004) 561-565

[8]     D. Gentry, G.T. Pancio, and J.J. Weers, Use of olefinic imines to scavenge sulfur species, US Patent 5,567,213. Oct 22 1996.

[9]     G. Westlund and D. Weller, Aromatic imine compounds for use as sulfide scavengers, US Patent 7,985,881 B2. July 26 2011

[10]    A. Murugesan et al., Kinetic and thermodynamic studies on the removal of Zn2+ and Ni2+ from their aqueous solution using poly(phenylthiourea)imine, Chemical Engineering Journal 197 (2012) 368-378

[11]    A. Simion et al., Synthesis of imines, diimines and macrocyclic diimines as possible ligands, in aqueous solution, J. Chem. Soc. 1 (2001) 2071-2078

[12]    M.M.A.R. Moustafa, A.C. Stevens, B.P. Machin, and B.L. Pagenkopf, Formal [4 + 2] Cycloaddition of Alkoxy-Substituted Donor-Acceptor Cyclobutanes and Aldehydes Catalyzed by Yb(OTf)3, Organic Letters 12 (21) (2010) 4736-4738

[13]    V. Saggiomo and U. Lüning, On the formation of imines in water—a comparison, Tetrahedron Letters 50 (2009) 4663-4665

[14]    E. Moulin, G. Cormos, and N. Giuseppone, Dynamic combinatorial chemistry as a tool for the design of functional materials and devices, Chem. Soc. Rev. 41 (2012) 1031-1049

[15]    V. Saggiomo and U. Luning, Remarkable Stability of Imino Macrocycles in Water, Eur. J. Org. Chem. 25 (2008) 4329-4333

[16]    Y. Bekdemir and K. Efil, Microwave Assisted Solvent Free Synthesis of Some Imine Derivatives, Organic Chemistry International 2014 (2014) Article ID 816487

[17]    A.N. Phan and A.P. Harvey, Characterisation of mesoscale oscillatory helical baffled reactor - Experimental approach, Chemical Engineering Journal 180 (2012) 229-236

[18]    J.P. Solano, R. Herrero, S. Espin, A.N. Phan, and A.P. Harvey, Numerical study of the flow pattern and heat transfer enhancement in oscillatory baffled reactors with helical coil inserts, Chemical Engineering Research and Design 90 (2012) 732-742

[19]    A.N. Phan, A.P. Harvey, and M. Rawcliffe, Continuous screening of base-catalysed biodiesel production using New designs of mesoscale oscillatory baffled reactors, Fuel Processing Technology 92 (2011) 1560-1567

[20]   P. Atkins and J. De Paulu, Physical Chemistry. 9th ed. Oxford: Oxford University Press, 2010

[21]   F.R. Mohd-Rasdi, A.N. Phan, and Harvey. A.P., Rapid determination of reaction order and rate constants of an imine synthesis reaction using a mesoscale oscillatory baffled reactor, Chemical Engineering Journal 222 (2013) 282-291

[22]   M.R. Mackley and P. Stonestreet, Heat transfer and associated energy dissipation for oscillatory flow in baffled tubes, Chemical Engineering Science 50 (14) (1995) 2211-2224

[23]   D.A. Reay and P.A. Kew, Heat Pipes: Theory, Design and Applications. 5th ed. Butterworth Heinemann, 2006

[24]   P. Geladi and B.R. Kowalski, Partial least squares regression: A tutorial, Analytica Chmica Acta 185 (1986) 1-17

[25]   Anon, Heat pipes - performance of capillary-driven designs, Engineering Sciences Data Unit (EDSU), London, Data Item No. 79012, 1979

[26]   Anon, Heat Pipes - Performance of two-phase closed thermosyphons, Engineering Sciences Data Unit (EDSU), Data Item No. 81038, 1983

[27]   K. Han and D.H. Cho, A comparison of the heat transfer performance of thermosyphon using a straight groove and a helical groove, Journal of Mechanical Science and Technology (KSME Int. J.) 19 (2005) 2296-2302